



Preparation and characterization of iron–molybdate thin films

J.J. Uhlrich^a, J. Sainio^{a,1}, Y. Lei^{a,2}, D. Edwards^b, R. Davies^b, M. Bowker^b, S. Shaikhutdinov^{a,*}, H.-J. Freund^a

^a Abteilung Chemische Physik, Fritz-Haber-Institut der Max-Planck-Gesellschaft, Faradayweg 4–6, 14195 Berlin, Germany

^b Wolfson Nanoscience Lab and Cardiff Catalysis Institute, Cardiff University, Cardiff CF10 3AT, Wales, UK

ARTICLE INFO

Article history:

Received 17 January 2011

Accepted 20 May 2011

Available online 27 May 2011

Keywords:

Iron–molybdates

Thin films

Scanning tunneling microscopy

Infrared spectroscopy

ABSTRACT

Mixed Fe–Mo oxides are used in industrial catalytic processes of selective oxidation of methanol to formaldehyde. For better understanding of the structure–reactivity relationships of these catalysts we aim to prepare well-ordered iron–molybdate thin films as model catalysts. Here we have studied Mo deposition onto Fe₃O₄ (111) thin films produced on Pt(111) as a function of Mo coverage and annealing temperature using LEED, AES, STM and IRAS. At low temperatures, the iron oxide film is covered by Mo=O terminated molybdena nanoparticles. Upon oxidation at elevated temperatures (T>900 K), Mo species migrate into the film and form new bonds with oxygen in the film. The resulting films maintain the crystal structure of Fe₃O₄, and the surface undergoes a ($\sqrt{3} \times \sqrt{3}$)R30° reconstruction. The structure is rationalized in terms of Fe substitution by Mo in the surface layers.

© 2011 Elsevier B.V. All rights reserved.

1. Introduction

Fe–Mo oxide catalysts are commercially used for large-scale production of formaldehyde by the partial oxidation of methanol in an excess of oxygen (air) at relatively low temperatures, i.e. 350–450 °C. It has been established that industrial catalysts are iron–molybdates, Fe₂(MoO₄)₃, with an excess of MoO₃ [1–5]. The primary function of having molybdena in excess is most likely to replenish molybdenum which may sublime at elevated temperatures and lead to the formation of iron oxide-rich phases which favor total oxidation [2,6–8]. The identity of the active site for the partial oxidation of methanol is still a topic of current research, where some consider the stoichiometric Fe₂(MoO₄)₃ phase to act alone as the active phase, while others suggest that a molybdenum-rich phase is necessary in order to achieve a high activity and selectivity for formaldehyde production [2–4,9–12]. In a recent study aberration-corrected electron microscopy was applied to show that the surface layer of the catalyst is Mo rich [13–15], and is likely to consist of only Mo. This was recently confirmed using a variety of techniques, but especially high-resolution transmission electron microscopy [16]. This dominance of the surface by Mo is very important because this leads to high selectivity performance. It was shown that when Fe is present in the surface layers, the higher oxidation products, CO and CO₂, are formed [13–15], and that CO₂ is the dominant product for iron oxide surfaces. This appears to be due to the nature of the surface intermediates formed

on the two types of surface: Methoxy dominates on MoO₃, and decomposes in TPD to yield formaldehyde, whereas on iron oxide the formate species is produced, which is already over-oxidized with respect to formaldehyde formation [13–15].

In order to further our understanding of this particular mixed oxide system, we have studied the interaction of Mo deposited onto Fe₃O₄ and the structural evolution of this system at elevated temperatures which in turn leads to the formation of thin Fe–Mo oxide films. It should be noted that surface science studies of mixed oxides are a topic of current research, where atomic insight on the surfaces of mixed oxides is not commonly observed and remains of high interest in both catalysis and surface science in general (see, for instance, [17–19]). We intend to go on to investigate the reactive properties of these Fe–Mo oxide films, using them as model catalysts for the selective oxidation of methanol to formaldehyde. This work is part of our long-standing research activity in modeling oxidation catalysts (see, for instance, [18,20–22]). Using well-defined, metal-supported thin films can provide important information on the atomic structure of catalyst active sites. By taking advantage of the capabilities of modern surface science techniques, we take the next step towards an understanding of the atomic structure of the active site on the iron molybdate catalyst.

2. Experimental section

The experiments were performed in two separate ultrahigh vacuum (UHV) chambers with base pressures $\sim 5 \times 10^{-10}$ mbar. One chamber is equipped with an IR spectrometer (Bruker IFS 66/vs), a differentially pumped quadrupole mass spectrometer (Hiden HAL 201), and a low energy electron diffraction/Auger electron spectroscopy (LEED/AES, from Specs). The Pt (111) crystal (9 mm in diameter, 1.5 mm in

* Corresponding author. Tel.: +49 30 8413 4114; fax: +49 30 8413 4105.

E-mail address: shaikhutdinov@fhi-berlin.mpg.de (S. Shaikhutdinov).

¹ Present address: Department of Applied Physics, Aalto University School of Science and Technology, FI-00076 AALTO, Finland.

² Present address: Energy Systems Division, Argonne National Laboratory, Argonne, IL 60439, USA.

thickness) is spot-welded to two parallel Ta wires which are in turn welded to two Ta rods used for resistive heating and also for cooling by filling a manipulator tube with liquid nitrogen. The temperature is measured by a chromel-alumel thermocouple spot-welded to the backside of the crystal.

The second chamber houses a STM and LEED/AES (all from Omicron). The Pt(111) crystal, mounted to a Pt sample holder, can be heated by electron bombardment from the backside through the hole in the sample holder. The temperature is measured by a chromel-alumel thermocouple spot-welded to the edge of the crystal.

The Pt(111) single crystal was cleaned by repeated cycles of 1.5 keV Ar⁺ sputtering and UHV annealing at 1300 K. The Fe₃O₄(111) films were grown by first depositing the FeO(111) layer, which was in turn grown by deposition of one monolayer (ML) (1 ML corresponds to 1.5×10^{15} at/cm²) of Fe at 300 K and oxidation at 1000 K in 10^{-6} mbar O₂ for 2 min. The ~10 nm thick Fe₃O₄(111) films were grown on top of this FeO transition layer by four repeated cycles of ~5 ML Fe deposition and oxidation. After each deposition step at 300 K, the deposited layer was oxidized in 10^{-6} mbar O₂ at 950 K for 5 min with the final oxidation step at 1000 K for 10 min [23,24]. The presence of Fe₃O₄(111) was verified by the observation of the characteristic LEED pattern, where the pattern was uniformly sharp with a low background over the entire surface. Iron and molybdenum (both 99.95%, from Goodfellow) were deposited using e-beam assisted evaporators (Focus EFM3, Omicron). The metal (Fe and Mo) coverage was measured by STM for structural studies, while a quartz microbalance was employed for samples used in IRAS studies. This may cause deviation in the absolute numbers for Mo coverages in the two experimental setups. Typical deposition rates of Fe and Mo were of 0.5 Å/min. The cleanliness of the film (particularly with respect to

carbon) was verified by AES, where the carbon level was found to be below the detection limit of the instrumentation.

3. Results

3.1. LEED and STM study

Fig. 1 shows STM images of Fe₃O₄(111) films with 0.2 ML (a,b) and 2 ML (c and d) of Mo deposited at 300 K in UHV. Well-ordered morphology of the films is clearly seen on the large-scale STM images, where wide terraces are separated by the monoatomic steps running along the main crystallographic directions. The inset in Fig. 1a shows a characteristic LEED pattern of the Fe₃O₄(111) surface which gradually attenuates upon increasing Mo coverage. At the 0.2 ML coverage, randomly distributed particles of 3–4 Å in height and ~1 nm in diameter are observed (see Fig. 1b). The hexagonal lattice of atomic protrusions with a ~6 Å periodicity, characteristic for the clean Fe₃O₄(111) surface, is also visible between the particles. Note, that some atomic size features on this image were present on the films prior to the Mo deposition, and tentatively assigned to adsorbed species from the vacuum background. Upon increasing coverage to 2 ML, the particles grow in size up to 3 nm in diameter and 3–4 Å in height as shown in Fig. 1d.

The Mo/Fe₃O₄(111) films were annealed in $1-10^{-6}$ mbar O₂ by increasing temperature stepwise until an ordered LEED pattern appeared. No ordered structures were observed below 900 K, except for submonolayer Mo coverages where the diffuse (1×1) pattern of the underlying Fe₃O₄ substrate becomes sharper on heating. Correspondingly, AES study revealed Mo depletion at the surface upon annealing above 700 K.

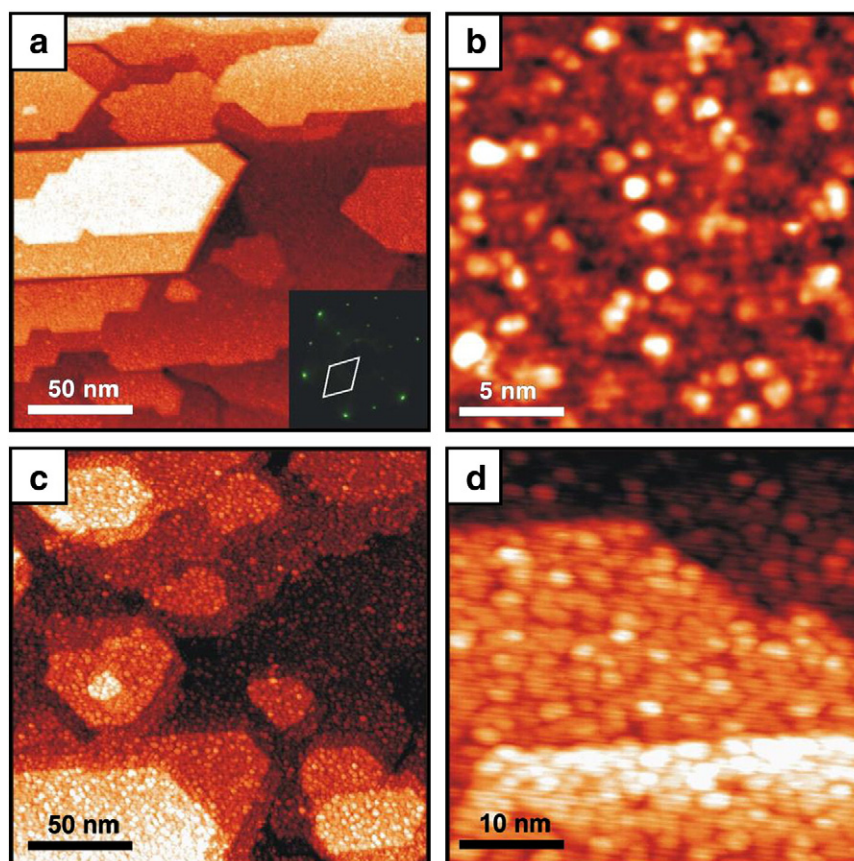


Fig. 1. STM images of 0.2 ML (a,b) and 2 ML (c,d) of Mo deposited on Fe₃O₄(111) film in UHV at 300 K. Tunneling bias and current are 2 V and 0.13 nA, respectively, for all images. As an inset in (a), the LEED pattern of Fe₃O₄ is shown, with the (1×1) unit cell corresponding to a periodicity of 5.94 Å.

Fig. 2 shows STM images of 1 ML Mo/Fe₃O₄(111) annealed in 10⁻⁶ mbar O₂ at 900 K for 5 min. In contrast to the original films showing well-oriented step edges, Mo-doped films expose domains (“grains”) separated by nm-wide narrow trenches of ~8 Å in depth. Within each domain, atomically flat terraces are separated by steps of ~5.5 Å in height, i.e., considerably higher as compared to the clean Fe₃O₄(111) films (~4.5 Å). In addition, the step edges are rather roundish and no longer aligned with the crystal orientation. LEED inspection of the resulting surface revealed a Fe₃O₄(111) – (√3 × √3)R30° structure (see the inset in Fig. 2a). The atomically resolved STM images (Fig. 2b) show the unit cell formed by tripod-like protrusions, in turn consisting of three protrusions with a 6 Å spacing as shown in the inset in Fig. 2b. There are also surface point defects, which appear as depressed tripods that show inverted symmetry with respect to the tripods surrounding the defect (inset in Fig. 2b). In addition, line defects are observed between the terraces of the same level, which are likely decorated by MoO_x species (see the protruding line in Fig. 2b).

The observed STM contrast on the Mo-doped surfaces strongly depended on bias. Fig. 3 shows two STM images of the same surface at different bias polarity. The tripod protrusions and point defects are clearly seen in the STM image obtained at –1.2 V (Fig. 3a). Several domains, coexisting on the same terrace and shifted by a half of lattice with respect to each other, are highlighted by the dashed lines. In addition, differently oriented protruding “dimers” are often observed in the vicinity of the point defects. Meanwhile, the defects are apparently missing in the STM image (Fig. 3b) obtained at +1.2 V, and the triple protrusions are recognizable, but not nearly as well-resolved. The atomic protrusions on both images form a close-packed lattice with a 6 Å periodicity as in the pristine Fe₃O₄ (111) film. In this

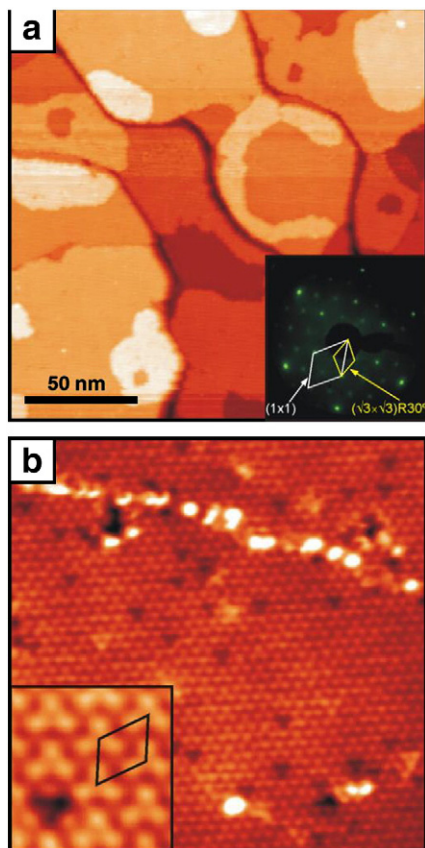


Fig. 2. STM images of 1 ML Mo/Fe₃O₄(111) annealed in 10⁻⁶ mbar O₂ at 900 K for 5 min. The inset in (a) shows the LEED pattern with the unit cells of the Fe₃O₄ substrate and the annealed Mo/Fe₃O₄(111) layer indicated. Size and tunneling conditions are (a) 180 nm × 180 nm, 1.5 V, 0.11 nA; (b) 25 nm × 25 nm (inset 3 nm × 3 nm), –1.67 V, 0.12 nA.

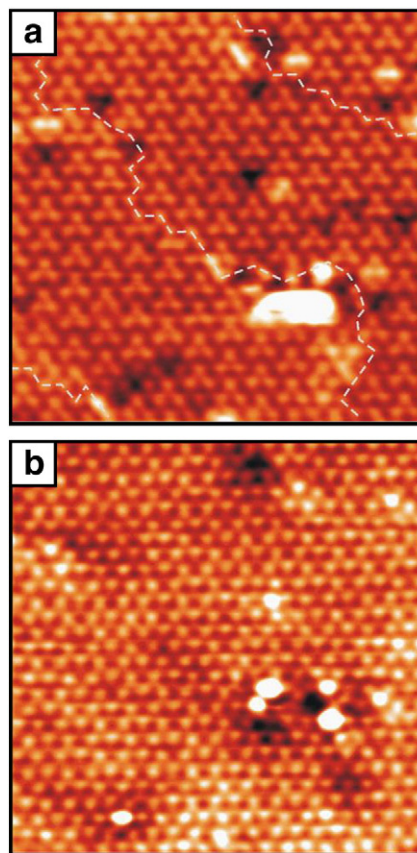


Fig. 3. STM images (15 nm × 15 nm) of 1 ML Mo/Fe₃O₄(111) annealed in 10⁻⁶ mbar O₂ at 900 K for 5 min showing bias dependence of the STM contrast. Tunneling bias is –1.2 V (a) and +1.2 V (b). Domain boundaries are highlighted by the dash lines.

study, almost indistinguishable ordered structures are observed for the 2 ML Mo/Fe₃O₄ (111) sample as judged by LEED and STM (not shown). Analogous structural behaviour has been observed previously by STM on the K-doped Fe₃O₄ surface [25].

3.2. IRAS study

The similarly prepared films were characterized by IRAS. Fig. 4a shows IRA-spectra obtained on Mo/Fe₃O₄ (111) surfaces as a function of Mo coverage deposited at 300 K in 10⁻⁶ mbar O₂. The spectra are referenced to the clean Fe₃O₄ (111) film. (Note, that the wave-like base line is resulted from increased surface roughness of the film and also transferring the sample to a Mo deposition stage between the measurements). The band at 1019 cm⁻¹ clearly develops upon increasing coverage and is characteristic for Mo=O stretching vibrations [26]. Therefore, it appears that the MoO_x particles formed upon deposition are Mo=O terminated.

Stepwise annealing of the 2 ML Mo/Fe₃O₄(111) sample in 10⁻⁶ mbar O₂ first leads to band sharpening and a shift of the more intense band to 1025 cm⁻¹ as shown in Fig. 4b. However, further increasing temperature above 700 K results in new spectral features at 945, 911, 780, 754 and 717 cm⁻¹ and disappearance of the 1025 cm⁻¹ band. This is more clearly seen in Fig. 5 for 1 ML and 2 ML Mo samples oxidized at 950 K in one step. Apparently, the IR peak intensity is independent of the Mo coverage, and this is in line with the STM and LEED results which revealed Fe₃O₄(111) – (√3 × √3)R30° structure for both, 1 ML and 2 ML coverages.

Further information on the film structure was obtained by performing isotopic experiments where ¹⁸O₂ was substituted for ¹⁶O₂. When ¹⁸O₂ was used for growth of the entire film, the IRAS

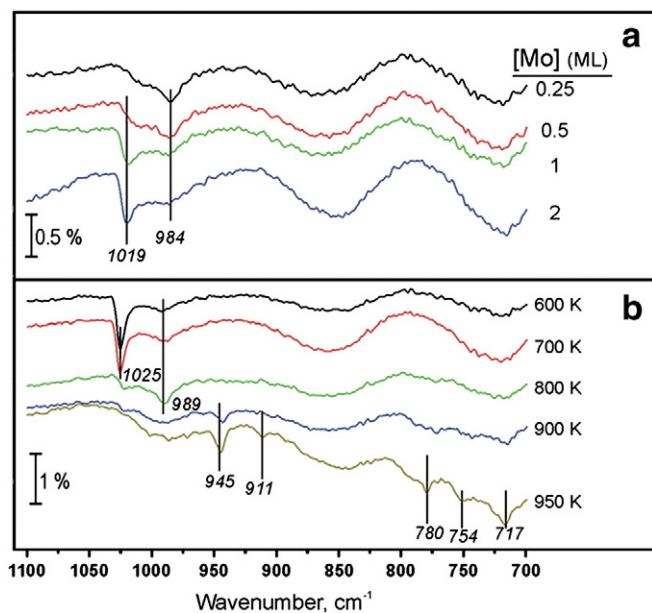


Fig. 4. IR spectra (a) of $\text{Mo}/\text{Fe}_3\text{O}_4(111)$ as a function of Mo coverage at 300 K, and (b) of 2 ML $\text{Mo}/\text{Fe}_3\text{O}_4(111)$ stepwise annealed to indicated temperature for 5 min. All spectra are recorded at 300 K and referenced to the spectrum of the clean $\text{Fe}_3\text{O}_4(111)$ film. The spectra are offset for clarity.

features (at 950–1030 cm^{-1} , see Fig. 4) were found to shift to lower wavenumbers by $\sim 50 \text{ cm}^{-1}$ (not shown). All frequency ratios were in excellent agreement with that predicted by the ratio of the Mo and O reduced masses for the isotopes (1.05) as well as previously published work for a thin oxide film formed on a Mo (112) substrate [26]. In contrast, when $^{16}\text{O}_2$ was used during Fe_3O_4 growth, and $^{18}\text{O}_2$ only for the subsequent Mo oxidation steps, the final vibrational bands remained unshifted from the $^{16}\text{O}_2$ values. The results suggest the formation of monoxo $\text{Mo}=\text{O}$ species upon Mo deposition in oxygen ambient. These molybdyl oxygens most likely recombine and desorb upon heating above 700 K, while Mo atoms form new bonds with O in the Fe_3O_4 films, ultimately forming $\text{Fe}_3\text{O}_4(111) - (\sqrt{3} \times \sqrt{3})\text{R}30^\circ$ structure revealed by LEED. Experiments with an equal mixture of $^{16}\text{O}_2$ and $^{18}\text{O}_2$ yielded an IR spectrum with rather broad isotopic bands overlapping, which exhibited a signal intensity too low for reliable interpretation.

4. Discussion

To rationalize the structure of well-ordered Mo-Fe oxide films by IRAS, we first address the results of studies using IR [1,3,5,26–32] and

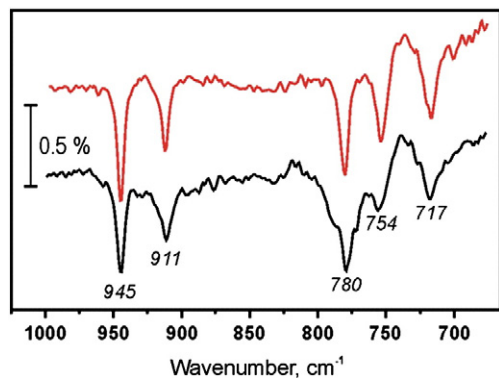


Fig. 5. IR spectra obtained for 1 ML (top) and 2 ML (bottom) $\text{Mo}/\text{Fe}_3\text{O}_4(111)$ surfaces oxidized at 950 K for 5 min. The spectra are recorded at 90 K and are offset for clarity.

Raman [4,33–44] spectroscopies of molybdenum oxide as well as iron molybdate systems. A summary of observed vibrational bands and their proposed assignments are presented in Table 1. A comprehensive review of Raman spectroscopy for supported molybdena species can be found in [45].

It is unlikely that there is MoO_3 formed in our model Fe–Mo oxide catalyst, due to the absence of vibrations at 1000 cm^{-1} and 820 cm^{-1} . The vibrations observed at 945 cm^{-1} and 911 cm^{-1} are somewhat lower in frequency than expected for the vibrations of molybdyl species in $\text{Fe}_2(\text{MoO}_4)_3$, showing that either there are no molybdyl species present on the surface, or that our film provides a unique chemical environment which shifts these vibrations to lower wavenumbers. The vibrational transition at 780 cm^{-1} has been reported previously as O–Mo–O in $\text{Fe}_2(\text{MoO}_4)_3$, where one study used this as a characteristic feature of $\text{Fe}_2(\text{MoO}_4)_3$ for determining the Fe/Mo ratio in the working catalyst [35]. The vibrations we observed at 751 cm^{-1} and 717 cm^{-1} have no specific assignments reported in Table 1. However, it has been reported that a broad feature is often observed in FTIR over the range of 700–900 cm^{-1} for the working iron molybdate catalyst [1,2]. These transitions were attributed to removal of the degeneracy with the complicated spectra originating from MoO_4 tetrahedra [1]. It is possible that the high degree of ordering in our film has enabled the resolution of these individual features. Upon reduction of the Fe–Mo oxide catalyst a number of additional phases have been observed, including $\text{Fe}_2(\text{MoO}_4)_3$, $\beta\text{-FeMoO}_4$, $\alpha\text{-FeMoO}_4$, $\text{FeMoO}_4\text{-II}$, and others [14,46]. In one previous study, Raman spectroscopy was performed separately on both $\text{Fe}_2(\text{MoO}_4)_3$ and $\beta\text{-FeMoO}_4$ phases [40]. Neither spectrum showed the peaks observed in this study between 700–800 cm^{-1} , providing no additional evidence that we have a reduced Fe–Mo oxide phase in this work.

We have looked at several hypotheses for an atomic model of the $\text{Fe}_3\text{O}_4(111) - (\sqrt{3} \times \sqrt{3})\text{R}30^\circ$ surface. Isotopic IRAS experiments, STM and AES results clearly show that, at elevated temperatures, Mo migrates into the iron oxide layers and forms new bonds with oxygen in the film. The resulting film maintains the crystal structure of Fe_3O_4 , as judged by LEED, although the surface undergoes a $(\sqrt{3} \times \sqrt{3})\text{R}30^\circ$ reconstruction. These findings suggest that most likely substitution of Mo atoms into the Fe_3O_4 lattice at Fe sites occurs upon annealing. Indeed, the substitutional alloys such as Fe_2MoO_4 (or more generally $\text{Fe}_{3-x}\text{Mo}_x\text{O}_4$ ($x=0-1$)) are known [46,47], which share the inverse spinel crystal structure with Fe_3O_4 .

In Fig. 6a, a cross view of the $\text{Fe}_3\text{O}_4(111)$ crystal structure is shown, where $1/4$ ML of tetrahedrally coordinated Fe (Fe_{tet}) over a close-packed oxygen layer was proposed as the topmost surface

Table 1

Vibrational bands and their proposed assignments for molybdena and iron molybdate systems.

Absorption band	Assignment	References
667 cm^{-1}	MoO_3 , O–Mo–O as.*	[33,34]
700–850 cm^{-1}	Mo–O–Mo in MoO_x tetrahedral Mo species in $\text{Fe}_2(\text{MoO}_4)_3$ octahedral M–O species	[35] [3,27,28] [28]
780 cm^{-1}	O–Mo–O as. in $\text{Fe}_2(\text{MoO}_4)_3$	[35,44]
816–860 cm^{-1}	MoO_3 , Mo=O sym.*, Mo–O–Mo as.	[28,29,31,33,35,44]
895 cm^{-1}	Mo–O–Mo in polymeric molybdate	[31]
915–920 cm^{-1}	Monomeric molybdate	[39]
	Mo=O as. in MoO_2	[29]
930–936 cm^{-1}	Mo=O sym., on $\text{Fe}_2(\text{MoO}_4)_3$	[27,44]
950–960 cm^{-1}	Polymeric molybdate, Mo=O sym. in MoO_2	[31,39,41] [29]
960–968 cm^{-1}	Mo=O in $\text{Fe}_2(\text{MoO}_4)_3$	[35,44]
	Fe–O–Mo as. in $\text{Fe}_2(\text{MoO}_4)_3$	[27,28]
990–1000 cm^{-1}	MoO_3 , Mo=O as	[3,28,31,33,35,44],
	MoO_4 sym. in $\text{Fe}_2(\text{MoO}_4)_3$	[27]
990–1026 cm^{-1}	M=O on Mo metal surfaces	[26,30]

*as.-asymmetric stretch; sym.-symmetric stretch.

termination [23,24]. The first and the second O-layers are separated by 3/4 ML of octahedrally coordinated Fe_{oct1} . The second and the third O-layers are separated by three more iron layers: 1/4 ML Fe_{tet2} , 1/4 ML Fe_{oct2} and 1/4 ML Fe_{tet1} . In order to form the Fe_2MoO_4 crystal structure, Mo ions would be substituted for half of the octahedral Fe in the lattice, where the precise positions of the Mo species are not reported in the literature [47]. However, in order to account for the experimentally deposited 1–2 ML of Mo solely in the surface unit, almost all of the Fe-sites would need to be substituted by Mo. It was experimentally observed that the LEED pattern of the surface relaxes back to the original pattern of Fe_3O_4 (111) upon annealing for extended times, presumably because the surface becomes too depleted of Mo to support the existence of the observed Fe–Mo-oxide phase. This indicates that this phase is relatively rich in molybdenum and may incorporate all or most of the 1–2 ML of Mo which was previously deposited. However, we cannot discount the possibility that some of the deposited Mo species sublime from the surface during oxidation or that the mixed Fe–Mo oxide phase extends very deeply within the film.

In Fig. 6b is shown the bulk structure of another iron molybdate, namely $\text{Fe}_2\text{Mo}_3\text{O}_8$, where the (0001) facet shares hexagonal surface structure with Fe_3O_4 (111) [48,49]. The surface unit cell of this compound ($a = 5.77 \text{ \AA}$, $b = 5.77 \text{ \AA}$) is very close to the value of 6.0 \AA measured on Fe_3O_4 (111). The structure could more easily account for the amount of deposited Mo without creating a thick surface layer. The structure of $\text{Fe}_2\text{Mo}_3\text{O}_8$ [48,49] shows a very similar ordering to Fe_2MoO_4 over several atomic layers, where the Fe_{oct1} sites are substituted with Mo, and there are only two Fe layers between the second and third O layers (compare Fig. 6a and b). Note, that all other iron–molybdate compounds, for which the crystal structure is reported, cannot exhibit surface with the trigonal (or hexagonal) symmetry and atomic periodicity as observed here for the films.

However, simple truncations of neither of the crystal structures shown in Fig. 6 would show the $(\sqrt{3} \times \sqrt{3})R30^\circ$ surface symmetry observed in LEED and STM, as both cation sites are distributed with 2×2 periodicity with respect to the oxygen layer. Therefore, in the next step of structure modelling, we generated structures which are (i) surface-enriched with Mo, and (ii) exhibit the $(\sqrt{3} \times \sqrt{3})R30^\circ$ surface periodicity. Fig. 7 shows the top view of such a hypothetical structure,

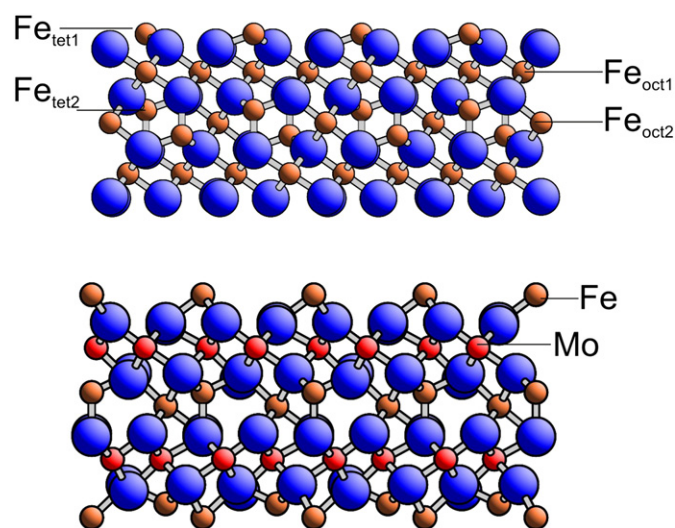


Fig. 6. (top) Side view of the Fe_3O_4 (111) surface where the blue and orange balls represent oxygen and iron respectively. The Fe_2MoO_4 crystal structure can be visualized by simply replacing half of the octahedral Fe ions by Mo. (bottom) side view of the $\text{Fe}_2\text{Mo}_3\text{O}_8$ (0001) surface where the red balls represent substituted molybdenum atoms.

where only the stacking of the first three layers as $\text{Mo}_{\text{tet}}\text{O}-\text{Mo}_{\text{oct}}\dots$ are shown, for clarity. Regardless of the surface termination (Mo or $\text{Mo}=\text{O}$), the vacancy could lead to an electronic enhancement from the Mo atoms in a subsequent layer below, effectively creating the triangular structures observed by STM (Fig. 3a). The topmost Mo ions could be molybdyl terminated, which would explain the relative inertness of the surface observed during STM imaging as compared to the Fe-terminated Fe_3O_4 (111) surface [50]. Molybdyl termination would also result in a higher, and possibly more favorable, oxidation state for the Mo ions on the surface. These species are typically imaged in STM as bright protrusions [51]. In the case an oxygen vacancy, molybdyl species could even tilt inward to compensate the charge, thus forming triangular features. The point defects, which mirror the protruding triangle (see inset in Fig. 3a), could then be explained by the lack of such an oxygen vacancy.

As mentioned above, the vibrations observed at 945 cm^{-1} and 911 cm^{-1} are somewhat lower in frequency than expected for molybdyl terminated surfaces, showing that the film probably provides a unique chemical environment which shifts these vibrations to lower wavenumbers. Certainly, additional experimental studies using photoelectron and x-ray absorption spectroscopies as well as computational input from theory could provide crucial information in refining the structure of iron molybdate films.

5. Conclusions

An ordered thin Fe–Mo oxide films were prepared by Mo deposition onto a thin Fe_3O_4 (111) film grown on Pt(111) and oxidation at elevated temperatures. During growth, the films were studied as a function of Mo coverage and annealing temperature in order to understand the early stages of structure formation. STM results showed atomic resolution of the mixed oxide phase, with ordered tripod species on the surface showing a periodicity of $\sim 10 \text{ \AA}$, consistent with the Fe_3O_4 (111) – $(\sqrt{3} \times \sqrt{3})R30^\circ$ structure observed by LEED. Five characteristic vibrational transitions were observed using IRAS to serve as a chemical fingerprint of the surface species on the Fe–Mo mixed oxide. A crystalline model is proposed where Mo is substituted for Fe in the surface layers and oxygen vacancies account for the periodicity observed by LEED and STM.

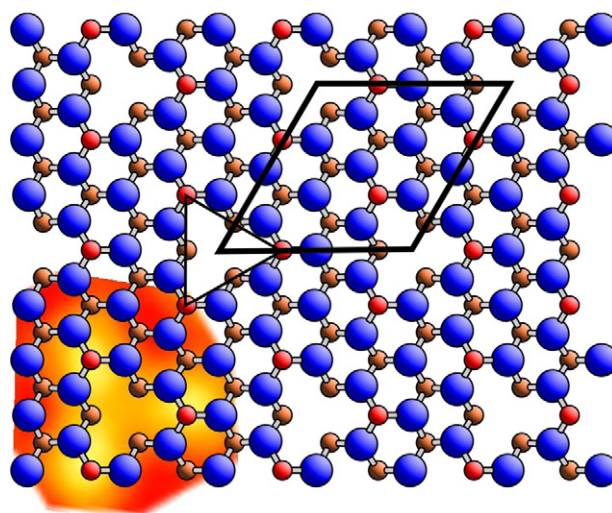


Fig. 7. Top view showing the first three atomic layers for the proposed structure of the Fe–Mo oxide film. The triangle and unit cell are indicated to compare with $(\sqrt{3} \times \sqrt{3})R30^\circ$ structure observed by STM in Fig. 3, where the triangular contrast observed by STM is directly compared with the crystalline model at the bottom left. Here, both red and orange atoms represent molybdenum atoms, where the different colors help to visualize the different atomic layers.

Acknowledgements

We acknowledge support from the Deutsche Forschungsgemeinschaft (DFG) through SFB546 (“Structure and reactivity of transition metal oxides”) and the Fonds der Chemischen Industrie. We also acknowledge the support of EPSRC in the UK for providing funds for this collaboration through grant EP/E03974X/1, and to the Welsh Livery Association for support for Robert Davies. We gratefully acknowledge Prof. K. Hermann for assistance with the BALSAC software and the formulation of the crystalline model.

References

- [1] L.I. Abaulina, G.N. Kustova, R.F. Klevtsova, B.I. Popov, V.N. Bibin, V.A. Melekhina, V.N. Kolomiichuk, G.K. Borekov, *Kinet. Catal.* 17 (1976) 1126.
- [2] A.P.V. Soares, M.F. Portela, A. Kiennemann, *Catalysis Reviews* 47 (2004) 125.
- [3] A.P.V. Soares, M.F. Portela, A. Kiennemann, L. Hilaire, J.M.M. Millet, *Appl. Catal. A* 206 (2001) 221.
- [4] E. Soderhjelm, M.P. House, N. Cruise, J. Holmberg, M. Bowker, J.O. Bovin, A. Andersson, *Top. Catal.* 50 (2008) 145.
- [5] M.R. Sunkou, S. Mendioroz, J.L.G. Fierro, J.M. Palacios, A. Guerreroruiz, *J. Mater. Sci.* 30 (1995) 496.
- [6] N. Pernicone, *Catalysis Today* 11 (1991) 85.
- [7] B.I. Popov, V.N. Bibin, G.K. Borekov, *Kinet. Catal.* 17 (1976) 322.
- [8] A.P.V. Soares, M.F. Portela, A. Kiennemann, L. Hilaire, *Chemical Engineering Science* 58 (2003) 1315.
- [9] G. Fagherazzi, N. Pernicone, *J. Catal.* 16 (1970) 321.
- [10] N. Pernicone, *Cattech* 7 (2003) 196.
- [11] G. Alessandrini, L. Cairati, P. Forzatti, P.L. Villa, F. Trifirò, *Journal of the Less Common Metals* 54 (1977) 373.
- [12] M. Carbucicchio, F. Trifirò, *J. Catal.* 45 (1976) 77.
- [13] M. Bowker, R. Holroyd, A. Elliott, P. Morrall, A. Alouche, C. Entwistle, A. Toerncrona, *Catal. Lett.* 83 (2002) 165.
- [14] M.P. House, A.F. Carley, M. Bowker, *J. Catal.* 252 (2007) 88.
- [15] M.P. House, A.F. Carley, R. Echeverria-Valda, M. Bowker, *J. Phys. Chem. C* 112 (2008) 4333.
- [16] K. Routray, W. Zhou, C.J. Kiely, W. Grunert, I.E. Wachs, *J. Catal.* 275 (2010) 84.
- [17] I.E. Wachs, *Catalysis Today* 100 (2005) 79.
- [18] M. Baron, H.L. Abbott, O. Bondarchuk, D. Stacchiola, A. Uhl, S. Shaikhutdinov, H.-J. Freund, C. Popa, M.V. Ganduglia-Pirovano, J. Sauer, *Angew. Chem. Int. Ed.* 48 (2009) 8006.
- [19] J.A. Rodriguez, D. Stacchiola, *Phys. Chem. Chem. Phys.* 12 (2010) 9557.
- [20] H.-J. Freund, M. Bäumer, H. Kuhlenbeck, *Adv. Catal.* 45 (2000) 333.
- [21] Y. Romanyshyn, S. Guimond, H. Kuhlenbeck, S. Kaya, R.P. Blum, H. Niehus, S. Shaikhutdinov, V. Simic-Milosevic, N. Nilus, H.-J. Freund, M.V. Ganduglia-Pirovano, R. Fortrie, J. Dobler, J. Sauer, *Top. Catal.* 50 (2008) 106.
- [22] M. Bowker, P. Stone, R. Smith, E. Fourre, M. Ishii, N.H. de Leeuw, *Surf. Sci.* 600 (2006) 1973.
- [23] S.K. Shaikhutdinov, M. Ritter, X.-G. Wang, H. Over, W. Weiss, *Phys. Rev. B* 60 (1999) 11062.
- [24] W. Weiss, W. Ranke, *Prog. Surf. Sci.* 70 (2002) 1.
- [25] S.K. Shaikhutdinov, W. Weiss, R. Schlogl, *Appl. Surf. Sci.* 161 (2000) 497.
- [26] S. Kaya, J. Weissenrieder, D. Stacchiola, T.K. Todorova, M. Sierka, J. Sauer, S. Shaikhutdinov, H.-J. Freund, *Surf. Sci.* 602 (2008) 3338.
- [27] A.M. Beale, S.D.M. Jacques, E. Sacaliuc-Parvalescu, M.G. O'Brien, P. Barnes, B.M. Weckhuysen, *Applied Catalysis A* 363 (2009) 143.
- [28] A.A. Belhekar, S. Ayyappan, A.V. Ramaswamy, *J. Chem. Technol. Biotechnol.* 59 (1994) 395.
- [29] F.A. Cotton, R.M. Wing, *Inorg. Chem.* 4 (1965) 867.
- [30] F.C. Nart, S. Kelling, C.M. Friend, *J. Phys. Chem. B* 104 (2000) 3212.
- [31] S.R. Seyedmonir, S. Abdo, R.F. Howe, *J. Phys. Chem.* 86 (1982) 1233.
- [32] M.F. Zhou, L. Andrews, *J. Chem. Phys.* 111 (1999) 4230.
- [33] M. Dieterle, G. Mestl, *Phys. Chem. Chem. Phys.* 4 (2002) 822.
- [34] M. Dieterle, G. Weinberg, G. Mestl, *Phys. Chem. Chem. Phys.* 4 (2002) 812.
- [35] C.G. Hill, J.H. Wilson, *J. Mol. Catal.* 63 (1990) 65.
- [36] C.G. Hill, J.H. Wilson, *J. Mol. Catal.* 67 (1991) 57.
- [37] E.L. Lee, I.E. Wachs, *J. Phys. Chem. C* 112 (2008) 20418.
- [38] J. Leyrer, R. Margraf, E. Taglauer, H. Knözinger, *Surf. Sci.* 201 (1988) 603.
- [39] J. Leyrer, M.I. Zaki, H. Knözinger, *J. Phys. Chem.* 90 (1986) 4775.
- [40] S.S. Saleem, *Infrared Phys.* 27 (1987) 309.
- [41] B. Sombret, P. Dhamelincourt, F. Wallart, *J. Raman Spectrosc.* 9 (1980) 291.
- [42] P.A. Spevack, N.S. McIntyre, *J. Phys. Chem.* 97 (1993) 11020.
- [43] J.H. Wilson, C.G. Hill, J.A. Dumesic, *J. Mol. Catal.* 61 (1990) 333.
- [44] Q. Xu, G.Q. Jia, J. Zhang, Z.C. Feng, C. Li, *J. Phys. Chem. C* 112 (2008) 9387.
- [45] G. Mestl, T.K.K. Srinivasan, *Catal. Rev. Sci. Eng.* 40 (1998) 451.
- [46] J.C.J. Bart, N. Burriesci, A. Gennaro, M. Petrera, *Appl. Catal.* 7 (1983) 151.
- [47] M. Abe, M. Kawachi, S. Nomura, *J. Phys. Soc. Jpn.* 33 (1972) 1296.
- [48] Y. Lepage, P. Strobel, *Acta Crystallogr. Sect. B: Struct. Commun.* 38 (1982) 1265.
- [49] P. Strobel, Y. Lepage, S.P. McAlister, *J. Sol. State Chem.* 42 (1982) 242.
- [50] S. Shaikhutdinov, W. Weiss, *J. Mol. Catal. A* 158 (2000) 129.
- [51] S. Guimond, J.M. Sturm, D. Gobke, Y. Romanyshyn, M. Naschitzki, H. Kuhlenbeck, H.-J. Freund, *J. Phys. Chem. C* 112 (2008) 11835.